12th International Conference on Fracture Mechanics of Concrete and Concrete Structures
FraMCoS-12
B.L.A. Pichler, Ch. Hellmich, P. Preinstorfer (Eds)

https://doi.org/10.21012/FC12.1308
MS15-2:1

EXPERIMENTAL STUDY ON THE CONTRIBUTION OF FIBERS ON THE PUNCHING SHEAR CAPACITY OF PLAIN ECC SLABS

CHANG WU[*], YANLI SU[*], MINGWEN XU[*], CHENHUA JIN[†]

[*] Southeast university, School of civil engineering
Nanjing, 210096, China
e-mail: changwu@seu.edu.cn (C. WU)
e-mail: suyl@seu.edu.cn (Y. SU)
e-mail: 230248185@seu.edu.cn (M. XU)

[†] Jinling Institute of Technology, Schoo of Architectural Engineering
Nanjing 211169, China
e-mail: jinchenhua@jit.edu.cn (C. JIN)

Key words: Engineered cementitious composite, Slabs, Fiber volume fraction, Punching shear behavior, Load-bearing capacity

Abstract: This study aims at investigating the influence of fibers on the punching shear capacity of plain ECC slabs. An experimental investigation was conducted on the punching shear resistance of plain ECC slabs with varying fiber volume fractions (FVFs). A total of sixteen plain ECC slabs were cast and tested, each with dimensions of 300 mm in side length and 40 mm in thickness. All slabs were simply supported on a bespoke steel framework with eight supports and concentrically loaded through a circular steel column stub with dimensions of 66 mm in diameter and 30 mm in height. The experimental results revealed that the plain ECC slabs with FVFs of 1.0%, 1.5% and 2.0% were characterized by punching shear failure, while slabs featuring 0.5% FVF were governed by flexural failure. It can be concluded that increasing FVF enhances the flexural capacity of plain ECC slabs more significantly than their punching shear capacity. Moreover, increasing the fiber volume fraction resulted in an increase in both crack resistance and ultimate load-carrying capacity. Notably, the punching shear capacity of plain ECC slabs increased almost linearly with increasing fiber volume fractions.

1 INTRODUCTION

Engineered cementitious composite (ECC) is a high-performance construction material that emerged in the early 1990s through the pioneering efforts of Li [1-3]. A hallmark of ECC is its multiple cracking and tensile strain-hardening behavior, enabling it to achieve an ultimate tensile strain capacity ranging from 2% to 10% in direct tensile tests [4-12]. Consequently, plenty of studies have been devoted to exploring the potential of ECC as a substitute for traditional concrete, with the objective of enhancing the ductility, durability, and resilience of structural edifices [13-19].

A particularly promising application is the utilization of ECC in flat slab systems to fortify the punching shear capacity and alleviate the brittle failure commonly observed in concrete flat slabs. Research in this domain has seen a marked increase in recent years [20-29]. Nevertheless, existing studies have examined the contribution of the fibers' bridging effect on the punching shear behavior of ECC slabs inadequately. The failure mechanisms, critical punching shear crack angles, and energy absorption capabilities within plain ECC slabs

also remain to be fully elucidated.

In the present investigation, the impact of fibers on the punching shear capacity of plain ECC slabs was analyzed through experiments conducted on sixteen plain ECC slabs, each measuring 300 mm in side length and 40 mm in thickness. All slabs were supported on a custom-designed steel framework with eight supports and subjected to concentric loading via a circular steel column stub, 66 mm in diameter and 30 mm in height. The experimental findings could offer profound insights into the punching and flexural behavior of ECC slabs, thereby establishing a foundation for the design and advancement of flat systems reinforced with ECC.

2 EXPERIMENTAL PROGRAM

2.1 Text matrix and specimen fabrication

Sixteen plain ECC slabs were prepared and tested to evaluate their punching shear behavior. These slabs were categorized into four groups considering the fiber volume fractions, i.e., G2.0, G1.5, G1.0, and G0.5. For instance, the volume fraction of PE was 2% in Group G2.0 and four identical slabs were prepared for each group. All ECC slabs had the same dimensions with 300 mm in side length and 40 mm in thickness. The shear to depth ratio was kept constant at 1.0 to ensure that plain ECC slabs could undergo a punching shear failure, which can be concluded in the accompanying study [30]. In the specimen construction, the fresh ECC mixtures were cast in the prepared wooden formwork, and the tensile and compressive samples were prepared simultaneously. After casting, all specimens were covered with plastic film for 24 hours, then demolded and cured in air for 28 days.

2.2 Materials

The mix proportions for the ECC material used in this study are listed in Table 1. Four types of ECC were prepared, each with different fiber volume fractions of polyethylene (PE) fiber. The raw materials consisted of P.O. 42.5 cement, class I fly ash and quartz sand. Type I ordinary Portland cement was used and the quartz sand with a mesh size of 70-120 served as the fine aggregate. A high-efficiency superplasticizer was added to provide proper fluidity, which was provided by Subote New Materials Co., Ltd. Four volume fractions of PE fiber were used ranging from 0.5% to 2.0% in increments of 0.5%. PE fiber used in the test program had the tensile strength of 3 GPa and the elastic modulus of 116 GPa. The length and diameter of individual fiber were 12 mm and 24 μm, respectively.

Table 1: Mix proportion of ECC material in kg/m^3

Cement	305.39
Quartz sand	462.74
Water	359.13
Fly ash	997.23
Water reducer	1.53

Per JC/T 2461-2018, cubes with 100 mm×100 mm×100 mm were tested to measure the ECC's compressive strength, while dog-shaped samples were used to determine the tensile properties of ECC (see **Fig. 2a**). The compression test was performed using a 3000 kN hydraulic universal testing machine under force control at a rate of 0.5 MPa/s. The tensile test was directed by displacement via a 10 kN universal testing machine at a rate of 0.4 mm/min. Two linear variable differential transducers (LVDTs) were used to capture the longitudinal deformation of the central part (80 mm) of ECC dog-boned specimens. The average compressive strength of four types of ECC is presented in **Fig. 1**, and the tensile strain-stress curves are presented in **Fig. 2b**.

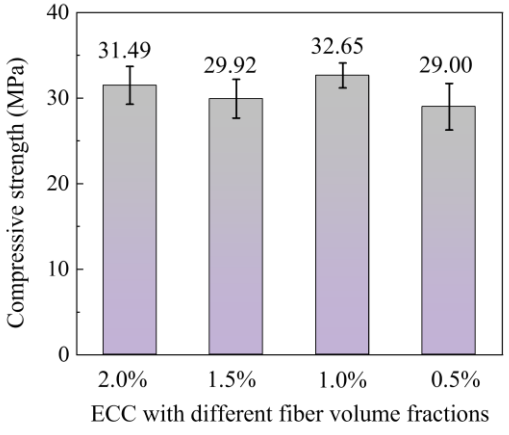

Figure 1: Average compressive strength.

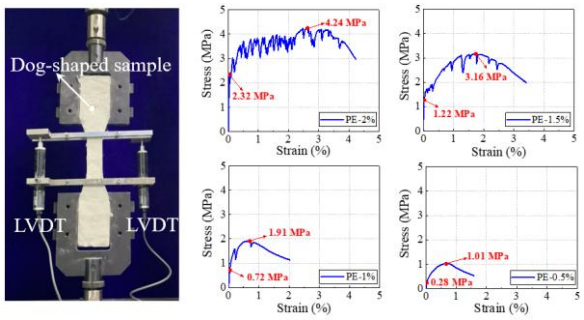

(a) (b)

Figure 2: The tensile testing and results of ECC material: (a) uniaxial tension test, and (b) tensile strain versus stress curves of ECC with different fiber volume fractions.

2.3 Test procedure and instrumentation

All plain ECC slabs were performed via an electronic universal testing machine with a bearing capacity of 100 kN, as presented in **Fig. 3**. The load was centrally applied to the slabs through a steel stub column measuring 66 mm in diameter and 30 mm in height. Each slab was simply supported on eight supports arranged on a bespoke steel framework and the configuration of the supporting also can be detected in **Fig. 3**. The diameter of the supports was 146 mm, which can be calculated as twice the slab's thickness plus the loading plate's diameter (66 mm). Fine sand was underneath the steel stub to ensure a vertical concentric loading. All slabs were tested at a constant loading rate of 0.5 mm/min. Deflection was measured at the center of the slabs using one LVDT, and data was recorded simultaneously with a DH3816N static testing system at a frequency of 1.0 Hz. The loading was continued until the applied load decreased approximately 80% of the peak load.

Figure 3: Loading setup and supporting configuration.

3 TEXT RESULTS AND DISCUSSION

3.1 Failure of specimen

The crack distribution and failure modes on the tensile and compressive sides of the plain ECC slabs are presented in **Fig. 4**. Generally, due to the small shear-depth ratio, the plain flat slab primarily exhibited behavior governed by punching shear resistance. From the photos of the examined slabs, it can be observed that punching shear failure occurred in Groups G2.0, G1.5 and G1.0, and flexural failure was observed for the examined slabs with the fiber volume fraction of 0.5%.

All slabs in Group G0.5, featuring 0.5% fiber fractions by volume, clearly exhibited the evidence of flexural failure at the ultimate load. The first visible flexural crack was observed in the center of the slab and rapidly propagated to the edges. As the load continued, more flexural cracks appeared on the tensile side of the slabs, exhibiting a radial pattern. In the later of the loading process, the width of flexural cracks became widened, and PE fibers were pulled out or ruptured within the crack channel, see **Fig. 4a**. Few circumferential cracks formed on the compressive side of plain ECC slabs, while no circumferential crack was observed at the tensile face during the whole loading process. In Group G0.5 with the fiber volume fraction of 0.5%, the failure of plain ECC slabs was primarily governed by the tensile flexural cracks.

For the remaining slabs in Groups G1.0, G1.5 and G2.0, they all failed in punching shear failure mode and exhibited in a similar manner with the crack propagation. The flexural crack first appeared on the tensile side of the slabs. As the load increased, the number of flexural cracks gradually increased and circumferential cracks formed underneath the steel tub column on the tensile face. The width of circumferential crack widened and developed as the main cracks, ultimately governing the failure of the plain ECC slabs. The punching line at the tensile face is labeled for the examined slabs in **Fig. 4a**. At the ultimate load, multiple flexural cracks can be observed on the tensile side of the slabs, and the concrete spalling was observed

around the steel column stub on the compressive face (**Fig. 4b**).

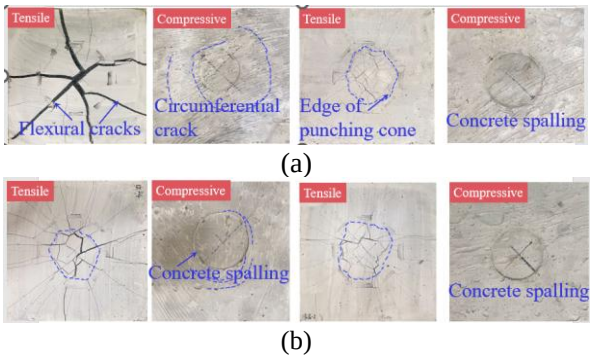

Figure 4: Crack distribution of plain ECC slabs: (a) tensile side and (b) compressive side.

3.2 Crack distribution

The plain ECC slabs were cut in half along the edge of slab to detect the critical punching shear failure surface and clarify the failure mechanism of slabs. The crack distributions at the ultimate load are marked with dashed lines of different colors, as shown in **Fig. 5**. It can be seen that the punching shear cracks were observed on the saw-cut section of all specimens, which were initiated from the edge of column stub and extended to the bottom side of the slabs within the supporting area. In Group G0.5, the flexural cracks exhibited the widen width and concrete crushing was observed on the top of slab, which revealed that Group G0.5 was characterized by the clear flexural failure mode. In the remaining specimens, obvious punching shear cone can be observed and the angle of punching shear failure surface was slightly greater than 45°. Only one flexural crack occurred in Group G1.5 and no flexural crack can be detected in Group G2.0, which can be concluded that pure punching shear failure mode occurred in plain ECC slabs with fiber volume fractions of 1.5% and 2.0%.

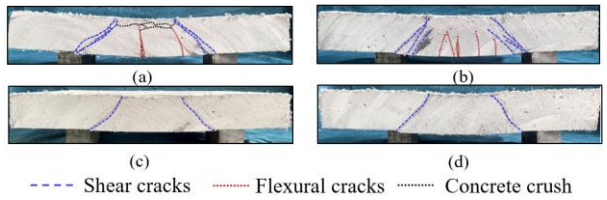

Figure 5: Crack distributions on the saw-cut section of slabs: (a) Group G0.5; (b) Group G1.0; (c) Group G1.0; and (d) Group G2.0.

3.3 Load and deflection responses

The load versus deflection curves of plain ECC slabs with different fiber volume fractions are presented in **Fig. 6**. The curves with the light color were the tested results of each slab and the curves with the deep color were the average values of four identical slabs. It can be seen that all curves exhibited ductile behavior due to the bridge effect of PE fiber. The overall trend of plain ECC slabs with different fiber volume fractions showed consistent regularity, and the loading process can be categorized into three stages as elastic stage (OA segment), cracking opening and stable expansion stage (AB segment), and failure stage (BC segment).

In the first stage, the deflection was linearly proportional to the applied load, and the stiffness was the largest in the entire loading process. At this stage, the load is borne by matrix without considering the effect of fibers. With the increasing applied load, the first flexural crack (P_A) occurred in the middle of the slab, and the curve entered into the second stage (AB segment). In this stage, the stiffness was obviously lower relative to the elastic stage with the generation of crack. PE fibers bridged the parts of the matrix where crack existed, thus the slabs did not quite the work and could still bear the external force. The load reached the energy required for the generation of new cracks and the number of cracks constantly increased with the increasing applied load. The slabs began to undergo steady-state multiple cracking. Multiple fine cracks formed on the tensile face, displaying a radial pattern. In Groups G1.0, G1.5 and G2.0, circumferential cracks also can be observed within the area underneath the steel stub column on the tensile side of the slab. Thereafter, the plain ECC slabs reached their maximum bearing capacity (P_B), marking the onset of the final failure stage. In this stage, few flexural and circumferential cracks occurred on the tensile side, and crack development was mainly characterized by increased width. The curve decreased slowly with the increasing deflection, exhibiting a clear ductile failure manner. The test was stopped until the applied load decreased to approximately 80% of the peak load, indicating

the failure of the examined slabs.

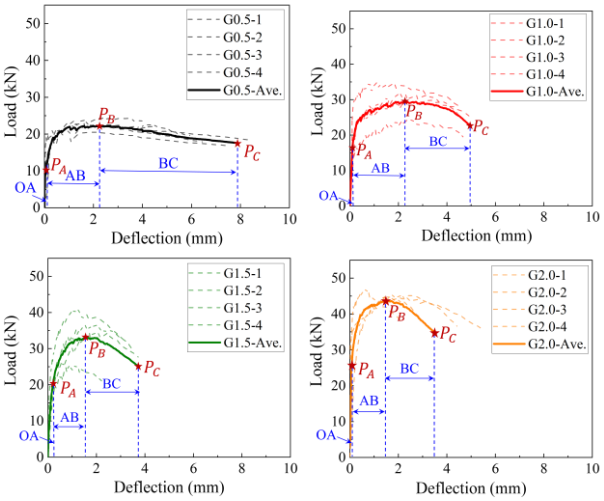

Figure 6: Load-deflection curves of each slab.

Table 2: Mix proportion of ECC material

Group	P_A (kN)	D_A (mm)	P_B (kN)	D_B (mm)	D_C (mm)
G0.5	9.91	0.05	22.63	2.39	7.84
G1.0	16.72	0.29	30.17	2.30	4.92
G1.5	21.75	0.19	34.31	1.54	3.73
G2.0	28.75	0.17	45.55	1.44	3.43

The average critical loads and corresponding deflections of plain ECC slabs are extracted and listed in **Table 2**. The ultimate load (P_C) was defined as the 80% of the peak load (P_B) in this study, and its value did not list in the table. It can be seen that increasing volume fraction of fiber led to an increase in the values of P_A and P_B, indicating that a higher fiber volume fraction positively affects crack load and bearing capacity of plain ECC slabs. For instance, the crack load and peak load of slabs in Group G1.0 were 68.72% and 33.32% higher, respectively, than those of in Group G0.5. Slabs in Group G2.0 experienced the highest bearing resistance, with a crack load of 28.75 kN and a peak load of values of 45.55 kN. The increased punching shear resistance of plain ECC slab is due to the PE fiber bridging cracks throughout the matrix and transferring tensile stress through the crack channel until fiber are pulled-out or ruptured. In addition, the ultimate deflection (D_C) of slabs in Group G0.5 was much larger relative to the rest of the slabs, which was attributed to the different failure modes. Plain ECC slabs in Group G0.5 experienced the clear flexural failure and exhibited the excellent ductile behavior, while punching shear occurred in Groups G1.0, G1.5 and G2.0.

3.4 Discussion

The relationship between fiber volume fraction and tensile peak stress (Fig. 7a) and punching shear resistance (Fig. 7b) is examined to identify trends and correlations. The tensile peak stress was determined through tensile testing of dog-shaped specimens, while the punching shear resistance was assessed using plain ECC slabs. In addition, a fitting curve is provided in the right panel of **Fig. 7**.

It can be seen from **Fig. 7a** that tensile peak stress of ECC materials with different fiber volume fractions exhibited minimal dispersion, revealing a notable trend towards higher peak stress for higher volume fraction of PE fiber. It is intuitive since a higher fiber volume fraction leads to an increase in bridge effect of fiber, thereby enhances the tensile strength of ECC. Through regression fitting, the relationship between tensile peak stress (y_1) and fiber volume fraction (x) can be expressed as $y_1=1.56x+0.28$.

Fig. 7b presents the relationship of fiber volume fraction and punching shear resistance of plain ECC slabs. The fiber volume fraction considerably increased punching shear capacity of plain ECC slabs, with the increase being directly proportional to the fiber volume. This enhancement is due to PE fibers bridging cracks through the matrix and transferring tensile stress through crack faces until the fibers are pulled-out or broken. It can be seen that plain ECC slabs in Group G1.5 exhibited significant variability, with one slab's capacity exceeding the average value by more than 30%, and this value should be discarded through the linear regression. The fitting curve between punching shear resistance (y_2) and fiber volume (x) of plain ECC slabs can be expressed as $y_2=15.17x+14.96$. In addition, the relationship between punching shear resistance (y_2) and peak stress (y_1) can be written as $y_2=9.6y_1+12.27$.

Due to the limitation of the conference paper length, more detailed discussion will be presented in a pull journal paper.

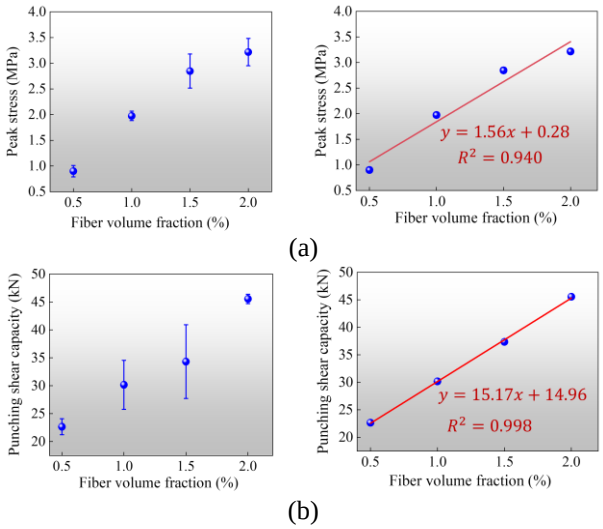

Figure 7: Relationship between fiber volume fraction and: (a) tensile peak stress of ECC and (b) punching shear capacity of plain ECC slabs.

4 CONCLUSIONS

Based on the experimental study, the following conclusions can be drawn:

(1) The experimental results revealed that plain ECC slabs with FVFs of 1.0%, 1.5%, and 2.0% exhibited punching shear failure, while slabs with a 0.5% FVF were characterized by flexural failure.

(2) Increasing the fiber volume fraction significantly enhanced the flexural capacity of the plain ECC slabs more than their punching shear capacity. Higher fiber volume fractions also led to increased crack resistance and ultimate load-carrying capacity of the slabs.

(3) The punching shear capacity of plain ECC slabs increased almost linearly with the increase in fiber volume fractions.

REFERENCES

[1] Li VC and Leung CKY. Steady-state and Multiple Cracking of Short Random Fiber Composites. Journal of Engineering Mechanics, 1992, 118(11):2246-2264.

[2] Li VC, Stang H, Krenchel H. Micromechanics of crack bridging in fiber-reinforced concrete. Materials and Structures, 1993, 26(162):486-494.

[3] Maalej M., Li VC, Hashida T. Effect of Fiber Rupture on Tensile Properties of Short Fiber Composites. Journal of Engineering Mechanics, 1995, 121(8):903-913.

[4] Yu K, Wang Y, Yu J, Xu S. A strain-hardening cementitious composites with the tensile capacity up to 8%. Construction and Building Materials, 2017, 137:410-419.

[5] Wu C, Pan Z, Su RKL, Leung CKY, Meng S. Seismic behavior of steel reinforced ECC columns under constant axial loading and reversed cyclic lateral loading. Materials and Structures, 2017, 50(1):78.

[6] Xu L, Pan J, Chen J. Mechanical Behavior of ECC and ECC/RC Composite Columns under Reversed Cyclic Loading. Journal of Materials in Civil Engineering, 2017, 29(9): 0001950.

[7] Ge W, Ashour AF, Cao D, Lu W, Gao P, Yu J, Ji X, Cai C. Experimental study on flexural behavior of ECC-concrete composite beams reinforced with FRP bars. Composite Structures, 2019, 208:454-465.

[8] Zhang D, Yu J, Wu HL, Jaworska B, Ellis BR, Li VC. Discontinuous micro fibers as intrinsic reinforcement for ductile Engineered Cementitious Composites (ECC). Composites: Part B, Engineering, 2020, 184(0):107741.

[9] Zhang P, Su Y, Liu Y, Gao D, Sheikh SA. Flexural behavior of GFRP reinforced concrete beams with CFRP grid-reinforced ECC stay-in-place formworks. Composite Structures, 2021, 277:114653.

[10] Yoo DY, Banthia N. High-performance strain-hardening cementitious composites with tensile strain capacity exceeding 4%: A review. Cement & Concrete Composites, 2022, 125:104325.

[11] Sun RJ, Han LB, Zhang HZ, Ge Z, Guan YH, Ling YF, Schlangen E, Šavija, B. Fatigue life and cracking characterization of engineered cementitious composites (ECC) under flexural cyclic load.

Construction and Building Materials, 2022, 335:127465.
[12] Su YL, Wu C, Shang JQ, Zhang P, Sheikh SA. Numerical and theoretical studies for the shear behavior of CFRP plate-ECC-concrete composite interface. Construction and Building Materials, 2023, 403:133156.
[13] Shwan HS, Hashim AR. Structural behavior of RC engineered cementitious composite (ECC) exterior beam–column joints under reversed cyclic loading. Construction and Building Materials, 2016, 107:226-234.
[14] Zheng Y, Zhang LF, Xia LP. Investigation of the behaviour of flexible and ductile ECC link slab reinforced with FRP. Construction and Building Materials, 2018, 166(0):694-711.
[15] Dong BQ, Pan JL. Mechanical behaviours of ECC-encased CFST composite column-RECC ring beam connections under axial and eccentric loading. Journal of Building Engineering, 2021,82:108226.
[16] Lim C, Jeong Y, Kim J, Kwon M. Experimental study of reinforced concrete beam-column joint retrofitted by CFRP grid with ECC and high strength mortar. Construction and Building Materials, 2022, 340:127694.
[17] Mohammad A, Esfahani MR. Effect of using Engineered Cementitious Composites (ECC) on failure behavior of flat slab-column connections. Structures, 2023, 47:2397-2407.
[18] Hariaravind G, Praveenkumar S, Sharmila S, Shanmugasundaram N. Behaviour of FRP-ECC-HSC composite stub columns under axial compression: Experimental and mathematical approach. Construction and Building Materials, 2023, 408:133707.
[19] Li S, Chan TM, Young B. Experimental investigation on axial compressive behavior of novel FRP-ECC-HSC composite short column. Composite Structures, 2023, 303:1-16.
[20] Ye B, Pan P, Xiao G, Han J, Zhang Y. Comparative study of reinforced-engineered cementitious composites and reinforced-concrete slab–column connections under a vertical monotonic load. Engineering Structures, 2021, 244:112740.
[21] Ye B, Pan P, Xiao G, Zhang Y, He Z. Experimental investigation on failure modes of RECC slab-column connections under concentric gravity loading. Engineering Structures, 2021, 230:111559.
[22] Aurélio S, Mário1 P, Sandra N. Experimental investigation on punching shear behaviour of RC-(R)UHPFRC composite flat slabs without transverse reinforcement. Engineering Structures, 2022, 255:113951.
[23] Huang XN, Li QH, Tong JZ, Xu SL, Lu YC. Punching shear behavior and strength prediction of UHTCC-enhanced RC slab-column joints. Engineering Structures, 2023, 286:116162.
[24] Huang XN, Tong JZ, Li QH, Xu SL. Numerical and analytical investigations on punching shear performance of UHTCC-enhanced RC slab-column joints. Journal of Building Engineering, 2023, 79:107900.
[25] Lampropoulos A, Tsioulou Q, Mina A, Nicolaides D, Petrou M. Punching shear and flexural performance of ultra-high performance fibre reinforced concrete (UHPFRC) slabs. Engineering Structures, 2023, 281:115808.
[26] Yu ZX, Tong GS, Tong JZ, Huang XN, Li QH, Xu SL. Punching shear tests and design of UHTCC-enhanced RC slab-column joints with shear reinforcements. Magazine of concrete research, 2024.
[27] Le HA, Hieu P, Pham DD. Numerical Modelling of Punching Shear Behavior of UHPFRC Flat Slabs, Lecture Notes in Civil Engineering, 2024, 442:1487-1494.
[28] Zhang YT, Wan YF, Zhu DZ, Wu JH, Huang BF, Yang R. Quasi-static experimental study on RC slab-column connections partially replaced by high-strength and high-ductility PE-ECC. China Civil Engineering Journal, 2024.

[29] Deng XF, Lan DQ, Weng YH, Chen GL, Qian K. Study on punching shear resistance of slab-column connections with partial ECC replacement. Engineering Mechanics, 2024, 1-13.
[30] Su YL, Wang XR, Wu C, Xu MW, Jin CH. Experimental investigation of flexural and punching behavior for plain PE-ECC slabs with different fiber volume fractions and span-depth ratios. Construction and Building Materials, 441, 2024, 137502.